

1 **U(VI) Binding onto Electrospun Polymers Functionalized with Phosphonate**

2 **Surfactants**

3 *Nabil Shaikh<sup>1</sup>, Jiajie Qian<sup>2</sup>, Sewoon Kim<sup>2</sup>, Hoa Phan<sup>3</sup>, Juan S. Lezama-Pacheco<sup>4</sup>, Abdul-Mehdi*  
4 *S. Ali<sup>5</sup>, David M. Cwiertny<sup>2</sup>, Tori Z. Forbes<sup>3</sup>, Amanda J. Haes<sup>3</sup>, and José M. Cerrato<sup>1\*</sup>*

5 \*Corresponding email address: [jcerrato@unm.edu](mailto:jcerrato@unm.edu)

6 Telephone: (001) (505) 277-2722

7 Fax: (001) (505) 277-1988

8 <sup>1</sup> Department of Civil, Construction, & Environmental Engineering, MSC01 1070, University of  
9 New Mexico, Albuquerque, New Mexico 87131, USA

10 <sup>2</sup> Department of Civil and Environmental Engineering, University of Iowa, Iowa City, IA52242,  
11 USA

12 <sup>3</sup> Department of Chemistry, University of Iowa, Iowa City, IA 52242, USA

13 <sup>4</sup> Department of Environmental Earth System Science, Stanford University, Stanford, California  
14 94305, USA

15 <sup>5</sup> Department of Earth and Planetary Sciences, MSC03 2040, University of New Mexico,  
16 Albuquerque, New Mexico 87131, USA

17

18

19

20 **Abstract**

21 We previously observed that phosphonate functionalized electrospun nanofibers can  
22 uptake U(VI), making them promising materials for sensing and water treatment applications.  
23 Here, we investigate the optimal fabrication of these materials and their mechanism of U(VI)  
24 binding under the influence of environmentally relevant ions (e.g.,  $\text{Ca}^{2+}$  and  $\text{CO}_3^{2-}$ ). We found  
25 that U(VI) uptake was greatest on polyacrylonitrile (PAN) functionalized with longer-chain  
26 phosphonate surfactants (e.g., hexa- and octadecyl phosphonate; HDPA and ODP, A,  
27 respectively), which were better retained in the nanofiber after surface segregation. Subsequent  
28 uptake experiments to better understand specific solid-liquid interfacial interactions were carried  
29 out using 5 mg of HDPA-functionalized PAN mats with 10  $\mu\text{M}$  U at pH 6.8 in four systems with  
30 different combinations of solutions containing 5 mM calcium ( $\text{Ca}^{2+}$ ) and 5 mM bicarbonate  
31 ( $\text{HCO}_3^-$ ). U uptake was similar in control solutions containing no  $\text{Ca}^{2+}$  and  $\text{HCO}_3^-$  (resulting in  
32  $19 \pm 3\%$  U uptake), and in those containing only 5 mM  $\text{Ca}^{2+}$  (resulting in  $20 \pm 3\%$  U uptake). A  
33 decrease in U uptake ( $10 \pm 4\%$  U uptake) was observed in experiments with  $\text{HCO}_3^-$ , indicating  
34 that  $\text{UO}_2\text{-CO}_3$  complexes may increase uranium solubility. Results from shell-by-shell EXAFS  
35 fitting, aqueous extractions, and surface-enhanced Raman scattering (SERS) indicate that U is  
36 bound to phosphonate as a monodentate inner sphere surface complex to one of the hydroxyls in  
37 the phosphonate functional groups. New knowledge derived from this study on material  
38 fabrication and solid-liquid interfacial interactions will help to advance technologies for use in  
39 the *in-situ* detection and treatment of U in water.

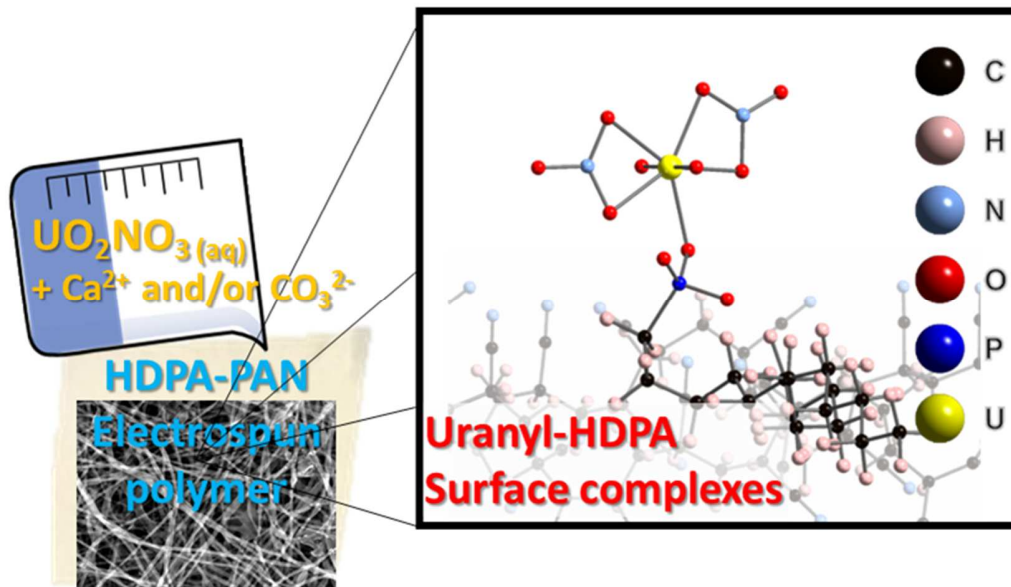
40

41 Keywords: phosphonate, electrospun polymer, uranium, spectroscopy, sensing

42

43 **Graphical Abstract**

44



45

46

47

48

## 49 **1 Introduction**

50 The transport of U(VI) caused by natural and anthropogenic processes can be concerning for  
51 surrounding communities and ecosystems<sup>1, 2</sup> due to the toxicological effects of U in humans,  
52 such as cancer and kidney failure.<sup>2, 3</sup> For water treatment applications, selective U uptake is  
53 possible by chelation with organic functional groups (e.g. phosphonate, quaternary ammonia,  
54 etc.) embedded in the surface of solid substrates.<sup>4, 5</sup> In particular, previous studies show up to  
55 three-fold increase in U uptake on phosphonate functionalized resins when compared to  
56 unfunctionalized materials, but the specific mechanisms affecting the solid-liquid interfacial  
57 interactions are not well understood.<sup>6-8</sup> Thus, fundamental understanding of U binding with  
58 phosphonate-functionalized materials is necessary for improving environmental remediation  
59 applications.

60 As a sorbent technology, electrospun polymers are ideal for promoting interfacial  
61 interactions due to their high surface to volume ratio and high porosity. Recent applications of  
62 electrospun polymers include passive sampling devices, materials for solid phase extraction,  
63 reactive filtration media, and platforms to concentrate dissolved targets for sensing  
64 applications.<sup>9-15</sup> PAN (polyacrylonitrile) is a common electrospun polymer with limited metal  
65 binding affinity via nitrile groups.<sup>16-20</sup> Uptake of U on PAN nanofibers can be enhanced by  
66 incorporating scavenging functional groups. In particular, phosphonates are an important  
67 chelating agent for U uptake due to strong binding over a wide pH range.<sup>21-24</sup> For example, we  
68 have previously shown that electrospun PAN nanofibers can be functionalized to improve U  
69 adsorption by simply incorporating surfactants with a phosphonate head group [e.g.,  
70 hexadecylphosphonate (HDPA)] directly into the sol-gel solution.<sup>9, 25</sup> This approach exploits the  
71 recognized ability of certain surfactants to surface segregate during electrospinning, a process

72 that results in the migration of the charged head of the surfactant to the polymer-air interface so  
73 as to minimize the free energy of interaction between the surfactant and the polymer support.<sup>26</sup>  
74 This produces PAN nanofibers that are surface-enriched in HDPAs binding sites that are suitable  
75 for U uptake under environmentally relevant conditions.

76 With the development of such functionalized materials for potential use in U treatment  
77 and/or sensing, there remains a need to elucidate the nature of species formed when U binds to  
78 surface-immobilized phosphonate moieties, particularly under conditions relevant to the intended  
79 application of the material. Although investigations with phosphonate-functionalized materials in  
80 complex, environmentally relevant aquatic matrixes remain limited, there are extensive studies  
81 that have considered the interaction of U with phosphonate ligands in solution that may prove  
82 helpful in understanding U uptake in heterogeneous systems.<sup>4, 27, 28</sup> For example, computational  
83 chemistry studies using thermodynamics and quantum mechanical calculations have shown that  
84 binding of uranyl with aqueous phosphonate functional groups can occur as monodentate (UO<sub>2</sub>-  
85 PO-) or binuclear bidentate (-PO-UO<sub>2</sub>-PO-) surface complexes, even in the presence of  
86 competing ligands such as inorganic carbonate and phosphate anions.<sup>27, 29-31</sup> For water treatment  
87 applications, carbonate is likely to be an important natural complexing agent that can react with  
88 U to form stable UO<sub>2</sub>-CO<sub>3</sub> aqueous complexes.<sup>30, 32</sup> Additionally, the presence of ternary U  
89 complexes involving a uranyl cation, carbonate anion, and alkaline earth metals like calcium  
90 (Ca) can influence the aqueous U(VI) speciation under circumneutral to alkaline pH conditions.<sup>7,  
91 33, 34</sup> The presence of soluble calcium ions in the mM range, which is typical of hard water, can  
92 also promote adsorption of phosphonate onto a model solid surface.<sup>35, 36</sup>

93 In this study, we expand upon our prior work with phosphonate-functionalized PAN  
94 nanofibers<sup>25</sup> to (i) optimize their synthesis with surface-segregating phosphonate surfactants to

95 promote U uptake and (ii) elucidate via spectroscopic methods the exact nature of the U species  
96 bound by surface-phosphonate moieties under conditions more representative of water treatment  
97 and sensing applications. Phosphonate surfactants are available with a range of alkyl chain  
98 lengths (from 10 to 18 carbon units), which we anticipate will affect both the extent of surface  
99 segregation and the retention of the surfactant in PAN. Accordingly, we first established the  
100 influence of alkyl chain length on U uptake in batch systems complemented by surface  
101 spectroscopic characterization (i.e., X-ray photoelectron spectroscopy). Then, through a series of  
102 batch uptake experiments in solutions containing calcium ( $\text{Ca}^{2+}$ ) and carbonate ( $\text{CO}_3^{2-}$ ) ions  
103 followed by selective chemical extraction of different bound U species, we probed changes in U  
104 binding mechanisms on phosphonate-functionalized PAN nanofibers using a suite of  
105 spectroscopic techniques (X-ray Photoelectron Spectroscopy, X-ray Absorption Spectroscopy,  
106 Raman Spectroscopy).

107 This study builds upon our prior work where such functionalized nanofiber materials  
108 have been used to concentrate dissolved U species prior to their quantification in water and  
109 biological fluids using Surface Enhanced Raman Scattering (SERS).<sup>4</sup> We contend there is need  
110 to develop additional U-specific substrates that might improve the sensitivity and selectivity of  
111 such sensing approaches, while also providing insights into dissolved U speciation. Therefore, in  
112 addition to improved insights into the mechanism of surface-segregation for the production of  
113 functionalized polymer nanofibers, novelty from this study is derived through the identification  
114 of specific processes that influence U binding to phosphonate-functionalized polymer  
115 membranes under environmentally relevant conditions. Although previous studies have utilized  
116 spectroscopic techniques to explore U uptake on minerals, there remains limited understanding  
117 on U uptake in complex environmental water matrixes by functionalized polymers.<sup>25, 37, 38</sup> Thus,

118 identification of the U uptake mechanisms herein will provide a framework to help advance the  
119 application of functionalized polymer nanofibers in various settings for U capture and  
120 concentration.<sup>39,40</sup>

121

## 122 **2 Materials and methods**

### 123 **2.1 Materials**

124 Polyacrylonitrile (PAN, mol wt. 150,000), dimethyl sulfoxide (DMSO), uranyl nitrate  
125 ( $\text{UO}_2(\text{NO}_3)_2 \cdot 6\text{H}_2\text{O}$ ), calcium chloride ( $\text{CaCl}_2 \cdot 2\text{H}_2\text{O}$ , ACS grade >99.5%), sodium bicarbonate  
126 ( $\text{NaHCO}_3$ , ACS grade >99.7%), gold(III) chloride ( $\text{HAuCl}_4 \cdot 3\text{H}_2\text{O}$ ), 6-mercaptophexanoic acid (6-  
127 MHA) were purchased from Sigma Aldrich. For studies with different chain length phosphonate  
128 surfactants, octadecyl phosphonic acid (ODPA, 97%), hexadecyl phosphonic acid (HDPA, 97%),  
129 tetradecyl phosphonic acid (TDPA, 98%), *n*-dodecyl phosphonic acid (DDPA, 97%) and decyl  
130 phosphonic acid (DPA, 97%) were also purchased from Sigma Aldrich and used as received.  
131 Sodium hydroxide (NaOH), hydrochloric acid (HCl), nitric acid ( $\text{HNO}_3$ ), and ethanol were  
132 purchased from Fisher Scientific. Ultrapure water ( $18.2 \text{ M}\Omega \text{ cm}^{-1}$ ) was used to prepare all the  
133 reagents. All glassware were cleaned with aqua regia (3:1 HCl/ $\text{HNO}_3$ ) and rinsed with ultrapure  
134 water before drying in the oven. *Caution:*  $\text{UO}_2(\text{NO}_3)_2 \cdot 6\text{H}_2\text{O}$  contains radioactive  $^{238}\text{U}$ , which is  
135 an alpha emitter, and like all radioactive materials, must be handled with care. These  
136 experiments were conducted by trained personnel in a licensed research facility with special  
137 safety precautions taken towards the handling, monitoring, and disposal of radioactive materials.

138

## 139 **2.2 Electrospun Nanofiber Synthesis**

140 Fabrication of the electrospun mat was performed on a custom designed electrospinner  
141 as detailed in our previous work.<sup>11, 25, 41</sup> As an example, the sol-gel for HDPA-functionalized  
142 materials was created by dissolving the parent PAN polymer (0.36 g) and HDPA surfactant  
143 (0.031 g) into 5 mL of dimethyl sulfoxide (DMSO) solvent. This corresponds to HDPA at 0.5  
144 wt.% relative to the overall sol gel mass (and an HDPA mole fraction of  $1.44 \times 10^{-3}$ ), which was  
145 the optimal loading for HDPA-functionalized materials that we previously reported.<sup>25</sup> For sol  
146 gels with other phosphonate surfactants of varying alkyl chain length, sol gels were prepared at  
147 the same mole fraction as the optimal HDPA formula ( $1.44 \times 10^{-3}$ ) so that all resulting  
148 nanofibers contained an equivalent amount of phosphonate moieties.

149 After their assembly, sol gel mixtures were placed on a rotating Thermomixer  
150 (Eppendorf) for 12 hours at 700 rpm and 60°C. This sol-gel is fed through a syringe pump at 0.5  
151 ml/hr and at 16-20% relative humidity to an electrospinner needle at 15 kV applied potential.  
152 This results in the formation of the electrospun nanofibers that are deposited on a ground  
153 collector surface rotating at 550 rpm. The mats were characterized using Electron Microscopy  
154 (SEM, **Figure S1**) and Infrared spectroscopy (ATR-FTIR, **Figure S2**). Surface area and pore  
155 volume measurements for select fibers were collected using N<sub>2</sub> Brunauer-Emmett-Teller (BET)  
156 sorption isotherm analysis (Quantachrome Nova 1200 Surface Area Analyzer), and all samples  
157 were degassed at 300°C for 3 hours prior to analysis.

158

## 159 **2.3 Uptake experiments**

160 *Influence of phosphonate surfactant chain length on U uptake studies.* U uptake  
161 experiments with DPA, DDPA, TDPA, HDPA, and ODPA followed procedures from our prior

162 work.<sup>25</sup> All systems contained a 20 mL solution of 1  $\mu\text{M}$  of uranyl nitrate [ $\text{UO}_2(\text{NO}_3)\cdot 6\text{H}_2\text{O}$ ] at  
163 pH 2 (Milli-Q Ultrapure water adjusted with 5 N  $\text{HNO}_3$ ) and 5 mg of phosphonate-functionalized  
164 nanofibers (0.25 g/L sorbent loading). This pH 2 solution was chosen for these experiments  
165 because of its relevance to treatment of U-contaminated acid mine drainage, and our prior work  
166 showing maximum removal of  $\text{U}^{6+}$  using HDP A-functionalized materials in 1  $\mu\text{M}$  total uranium  
167 systems. Reactors were allowed to react for 16 h (i.e., the duration we previously as sufficient to  
168 achieve sorption equilibrium), at which point the nanofiber mats were removed from solution  
169 and analyzed via liquid scintillation counting (LSC). Because we have previously found that  
170 surfactants can leach from electrospun nanofibers once submerged in aqueous solution,<sup>11</sup> uptake  
171 experiments were conducted both with as synthesized nanofibers and nanofibers that were  
172 extensively washed with water prior to reaction. The washing procedure followed that used  
173 previously by our group,<sup>11, 25</sup> where 5 mg of a functionalized PAN mat was placed in a 50 mL  
174 conical vial with 10 mL of Milli-Q Ultrapure water. Vials were then mixed end over end for 24  
175 hours, and the water was exchanged three times over that interval.

176 *Mechanism of U uptake studies.* Batch experiment were performed to investigate the  
177 mechanism of uranium uptake on the polymer mat. The characteristics of spring and surface  
178 waters near mine waste sites in New Mexico and Arizona measured in previous studies had pH  
179 ranging from 6.8 to 8.2, alkalinity values from 100 to 430 mg/l as  $\text{CaCO}_3$ ,  $\text{Ca}^{2+}$  concentration  
180 between 30 to 280 mg/l and U concentration between 50 to 700  $\mu\text{g/l}$ .<sup>1, 32, 42</sup> Based on these field  
181 conditions, created U stock solutions for use in batch uptake experiments. The solutions were  
182 prepared in 18.2M $\Omega$  ultrapure water with 10  $\mu\text{M}$  uranyl nitrate [ $\text{UO}_2(\text{NO}_3)\cdot 6\text{H}_2\text{O}$ ] at pH 7.0  
183 (buffered with 0.1 M HEPES). Initial uptake experiments were performed by adding 20 mL of  
184 the U stock solutions with 5 mg HDP A electrospun polymer mat in a centrifuge tube for 16

185 hours and are referred to throughout this work as *HDPA+U reactor*. Additional experiments  
186 were conducted with 10  $\mu\text{M}$  U (uranyl nitrate), (i) 5 mM Ca (as  $\text{CaCl}_2$ ) referred as  
187 *HDPA+U+Ca reactor* (ii) 5 mM  $\text{CO}_3$  (as  $\text{NaHCO}_3$ ) (designated *HDPA+U+CO<sub>3</sub> reactor*) and  
188 (iii) 5 mM each of Ca and  $\text{CO}_3$  (*HDPA+U+Ca+CO<sub>3</sub> reactor*), together at pH 7.0 (Adjusted with  
189 HCl). Upon completion of reaction, the electrospun polymer mat were removed from the reactor,  
190 rinsed with deionized water, and prepared for solid analyses.

## 191 **2.4 Extraction experiments**

192 A set of experiments were conducted to evaluate U release from the polymer mats after  
193 the uptake experiments. A subsample of the reacted mats from the uptake experiment reactors  
194 were taken for extraction experiments, referred to as *reacted HDPA+U*, *reacted HDPA+U+Ca*,  
195 *reacted HDPA+U+CO<sub>3</sub>* and *reacted HDPA+U+Ca+CO<sub>3</sub>* mats. These mats were reacted with 15  
196 mL of either: (i) 1 M  $\text{MgCl}_2$  at room temperature at pH 7 for 1 hour to extract ion exchangeable  
197 species bound to the surface through ionic interactions or outer-sphere complexes,<sup>43, 44</sup> or (ii) 50  
198 mM  $\text{HCO}_3$  (pH 8.3) to extract adsorbed U as inner sphere and outer sphere surface complexed  
199 U.<sup>32, 42, 45</sup> These extractions were performed on a benchtop mixture rotating at 60 rpm for 12  
200 hours.

201

## 202 **2.5 Solid and Liquid Analyses**

203 The top 5 nm (near surface) of reacted and control (unreacted) polymer mats were  
204 analyzed using survey and high-resolution X-ray Photoelectron Spectroscopy scans for the  
205 spectroscopic features of U, C, O, P and N. This provides insights on the binding chemistry of  
206 organic groups with U. The changes in binding environment of U were observed using the U 4f  
207 high resolution scan. Spectra were collected from three different areas on each sample using a

208 Kratos Axis DLD Ultra XPS with a Mg K $\alpha$  source. XPS high resolution spectra was collected for  
209 U 4*f*, C 1*s*, N 1*s*, O 1*s*, and P 2*p* using step size of 0.1 eV and pass energy of 20.

210 X-ray Absorption Spectroscopy (XAS) analyses were conducted at the Stanford  
211 Synchrotron Radiation Lightsource (SSRL) at beam line 11-2 to identify changes in oxidation  
212 state (XANES) and molecular coordination (EXAFS) of U during these batch experiments. The  
213 EXAFS provides coordination number, and bond distances (eg. U-U, U-N and U-C) in the local  
214 molecular environment and help identify the surface complexes when compared to reference  
215 values. These references (U adsorbed ferrihydrite, liebigite and carnotite) were analyzed during  
216 the same beamtime. At least six scans were collected for each sample, and 3 scans for the  
217 references.

218 Surface Enhanced Raman Scattering (SERS) measurements were collected using a semi-  
219 homebuilt Raman microscope (Olympus BX51, Intevac ExamineR 785) with a 10x objective  
220 coupled to a solid-state laser with an excitation wavelength of 785 nm, integration time of 40  
221 seconds, spot size of 10  $\mu$ m, and power of ~15 mW. Gold nanostars were synthesized and  
222 functionalized using a modified protocol from previous papers (SI, text S1).<sup>4, 40</sup> Prior to analysis,  
223 samples were placed on a glass slide, hydrated using 30  $\mu$ L ultrapure water, and covered with a  
224 cover slip. Light pressure was applied to the cover slip to eliminate trapped air-bubbles. SERS  
225 spectra were randomly collected at 8-10 different spots across the mats. These signals were  
226 averaged then subtracted using an averaged SERS spectrum collected on HDPA PAN mats (with  
227 gold nanostars but without U). Integrated areas from 870-806  $\text{cm}^{-1}$  were calculated to determine  
228 relative abundance of uranyl species on *reacted HDPA+U* and *reacted HDPA+U+Ca* mats. For  
229 *reacted HDPA+U+CO<sub>3</sub>* and *reacted HDPA+U+Ca+CO<sub>3</sub> reacted*, integrated areas from 852-  
230 806  $\text{cm}^{-1}$  were calculated as SERS signals of uranyl.

231 For phosphonate alkyl chain length studies, the concentration of U sorbed on  
232 functionalized nanofibers at equilibrium was determined via LSC according to the  
233 methodologies provided in Johns et al.<sup>25</sup> For all other U uptake studies, a Perkin-Elmer Nexion  
234 300D inductively coupled plasma-mass spectrometer (ICP-MS) system was used to analyze the  
235 total U concentration in liquid samples from the reactor. Additionally, chemical equilibrium  
236 modelling for U aqueous speciation was carried out using Visual MINTEQ with inputs based on  
237 the experimental conditions used for this study.

238

### 239 **3 Results and Discussion**

#### 240 **3.1 Electrospun polymer characterization**

241 The electrospun polymers have a polymeric backbone with the surfactant present on the  
242 surface as ligands as confirmed by XPS survey scans (**Table 1**). The XPS survey scans for the  
243 synthesized HDPA (control) electrospun polymers exhibited 1.3% P on the surface and the  
244 presence of a peak at 134 eV region representing XPS P 2p confirms the presence of  
245 phosphonate on the near surface of the electrospun polymer. The ATR-FTIR spectra (SI, **Figure**  
246 **S2**) also shows the presence of P-O-H bonding on the HDPA-PAN control mat. The microscopy  
247 results (SI, **Figure S1**) indicate that the dimensions of the nanofibers were similar for all the  
248 control and reacted mats with the width of each nanofibers at 120 nm and these results confirm  
249 similar swelling of the fibers as reported previous studies.<sup>9, 25</sup>

250

#### 251 **3.2 Effect of phosphonate alkyl chain length on U uptake**

252 Results of U uptake studies using PAN functionalized with HPA (6), OPA (8), DPA (10),  
253 DDPA (12), TDPA (14), HDPA (16) and ODPA (18) are shown in **Figure 1**. Data shown for

254 each material was collected with surfactant-functionalized PAN that was washed extensively  
255 prior to contact with U-containing solutions. This washing was intentional so as to dislodge any  
256 loosely retained surfactant. For these washed materials, U uptake increased with increasing chain  
257 length. For all surfactants with alkyl chains less than 14 carbons (i.e., HPA, OPA, DPA, DDPA,  
258 and TPA), U uptake was only slightly greater than that observed in control experiments  
259 conducted with unfunctionalized PAN (dashed line in Figure 1). Far greater U uptake was  
260 observed for HDPA (~40% of total U in the system) and ODPA (near complete uptake of all U  
261 in the system). Notably, from SEM there were no obvious differences in the morphology of these  
262 materials (see **Figure S4**) that could also be used to rationalize observed trends in U uptake.

263 For comparison, we also explored U uptake on a select number of materials that were  
264 used in sorption experiments immediately after synthesis (i.e., without washing to remove any  
265 loosely retained surfactant). For these unwashed materials, U uptake was less in all cases, with  
266 DPA, DDPA, and TPA exhibiting U uptake no greater than that observed in controls with  
267 unfunctionalized PAN (dashed line in Figure 1; note: we presume uptake on unfunctionalized  
268 PAN is primarily due to interaction of the uranyl ion with electron-rich cyano groups within the  
269 polymer).<sup>17</sup> For unwashed mats containing HDPA and ODPA, U uptake was greater than that  
270 observed in controls but equal to (for HDPA) or less than (for ODPA) the degree of sorption  
271 observed with the corresponding washed materials.

272 We have previously found that integration of surfactants into electrospun polymers can  
273 promote pollutant uptake via two mechanisms: (i) when well retained inside the polymer (i.e.,  
274 surfactants retained after washing), charged surfactant head groups present on the nanofiber  
275 surface act as complexation sites for dissolved species; and/or (ii) when poorly retained inside  
276 the polymer (i.e., surfactants are lost to solution during washing), the release of surfactant into

277 the solution leaves behind pores that can increase the specific surface area of the polymer (i.e.,  
278 the surfactant acts as a porogen).<sup>11, 46</sup> Typically, we have observed the greatest improvements in  
279 sorption capacity when the surfactant is well-retained inside the polymer, allowing the charged  
280 surfactant head on or near the polymer surface to selectively bind dissolved targets of opposite  
281 charge. Increases in uptake resulting from the surfactant acting as a porogen are typically less,  
282 but depend on the extent of surface area created by the resulting pore space and the inherent  
283 binding activity of the substrate in which the pores are generated.

284         Based upon these prior experiences with surfactant-functionalized PAN, we attribute the  
285 trends in U uptake shown in Figure 1 to differences in the retention of phosphonate surfactants  
286 with different alkyl chain lengths within PAN nanofibers. We postulate that phosphonate  
287 surfactants with shorter chain lengths (all those with alkyl chain lengths less than 14-carbon  
288 TDPA) are poorly retained in PAN. Upon immersion in aqueous solution, we suspect that their  
289 release from PAN is near complete and occurs relatively quickly, consistent with our observation  
290 of foaming (indicative of surfactants) within our reactors during U uptake experiments with  
291 materials used immediately after synthesis (i.e., unwashed materials). Accordingly, the slight  
292 increase in U uptake observed for DPA, DDDPA, and TDPA after washing of these materials (see  
293 Figure 1) likely results from increases in pore volume and specific surface area of the PAN that  
294 are produced when the surfactant is lost into solution. Indeed, based upon N<sub>2</sub> BET adsorption  
295 isotherm analysis, we observed notable increases in the measured pore volumes for HPA (6  
296 carbons) and OPA (8 carbons) after our washing procedure to remove loosely bound surfactant  
297 (**Table S1**), consistent with their roles as porogens.<sup>11</sup>

298         In contrast for HDPA- and ODPA-functionalized materials, we hypothesize that their  
299 longer alkyl chains promote improved retention in the PAN, presumably through increased

300 physical entanglement and hydrophobic interactions between their longer alkyl chains and  
301 polymer. This helps to immobilize their phosphonate heads on or near the PAN surface, where  
302 they are available to promote U uptake to levels well above those observed for unfunctionalized  
303 PAN. This is consistent with the U uptake observed for both unwashed and washed types of  
304 these materials, and notably there was no statistically significant increase in pore volume or  
305 surface area for ODPA functionalized materials after washing (see Table S1).

306 Without an observable increase in surface area or pore volume for ODPA-functionalized  
307 materials after washing, the increase in U uptake observed for washed ODPA-functionalized  
308 nanofibers is not entirely understood. We note that XPS analysis of as synthesized, unwashed  
309 materials revealed that surface P concentration was actually lowest for ODPA, with the greatest  
310 surface P concentrations measured for materials with shorter chain surfactants (see inset to  
311 **Figure 1** and **Figure S3**). We are left to speculate that the increase in U uptake on ODPA-  
312 functionalized materials after washing may be due to the release of poorly retained ODPA that is  
313 loosely bound primarily on the PAN surface rather than the bulk of the material, thereby limiting  
314 pore formation. Indeed, we noticed a small degree of foaming during the washing of HDPA- and  
315 ODPA-containing materials, indicative that a small portion of surfactant was released into  
316 solution during our washing procedure. If primarily bound to the polymer surface, loosely  
317 retained ODPA could have an inhibitory effect on uptake of U by unwashed materials by  
318 blocking more well-retained phosphonate sites that persist in the washed materials. Such  
319 interference of loosely retained, surface-bound ODPA on as synthesized materials could also  
320 explain the relatively low surface P concentration measured by XPS on unwashed ODPA-  
321 functionalized PAN (with 18 carbon atoms for every one P atom in surface-associated ODPA  
322 molecule. For example, the atomic of abundance of P relative to carbon in ODPA ( $C_{18}H_{39}O_3P$ ) is

323 only ~5%, which would be expected to lower the P 2p intensity measured with XPS. Additional  
324 experimental work is necessary, however, to further explore the greater uptake of U on ODPA-  
325 functionalized materials after washing.

326

### 327 **3.3 Experiments probing U uptake**

328 All subsequent experiments exploring U uptake were conducted using HDPA-  
329 functionalized materials. Although ODPA-functionalized materials exhibited more U uptake  
330 capacity, it was also more difficult to reproducibly synthesize due to stability issues with the sol  
331 gel precursor. We also have previously investigated HDPA-functionalized materials, thus we had  
332 a greater understanding of its performance (e.g., pH-dependent U uptake) than ODPA-  
333 functionalized materials.

334 The results from the uptake experiments indicate that the interaction of U with carbonate  
335 and with a mixture of calcium and carbonate causes the inhibition of U uptake on the HDPA  
336 electrospun polymer. For example, lower U uptake was observed in the *HDPA+U+CO<sub>3</sub>* and  
337 *HDPA+U+Ca+CO<sub>3</sub>* reactors when compared to the reactors without CO<sub>3</sub> (**Figure 2**).  
338 Comparable U uptake was observed in the *HDPA+U* reactor ( $1.98 \pm 0.07$   $\mu\text{g U/mg mat}$ ) and in  
339 the *HDPA+U+Ca* reactor ( $1.96 \pm 0.37$   $\mu\text{g U/mg mat}$ ). This similarity in U uptake can be  
340 attributed to highly preferential sorption of U on HDPA resulting in limited cationic competition  
341 from Ca.<sup>8, 47</sup> The uptake in the *HDPA+U+CO<sub>3</sub>* reactors was  $1.14 \pm 0.22$   $\mu\text{gU/mg mat}$ ,  
342 corresponding to 39.4% decrease in U uptake compared to the *HDPA+U* reactor. The  
343 *HDPA+U+Ca+CO<sub>3</sub>* reactors had the least U uptake ( $0.35 \pm 0.24$   $\mu\text{g U/mg mat}$ ) which  
344 corresponds to 82% decrease when compared to the *HDPA+U* reactor. This decrease is  
345 comparable to that observed in other studies showing 70% decrease in U sorption on mineral

346 surfaces when Ca and CO<sub>3</sub> are present.<sup>48, 49</sup> Thus, the presence of co-occurring ions influences  
347 the U uptake into the HDPA mats, which may be attributed to changes in U aqueous  
348 complexation.

349 The formation of neutral or negatively charged uranyl-carbonate or ternary calcium-uranyl-  
350 carbonate aqueous complexes decreases the binding of U in the mats. Chemical equilibrium  
351 modelling was used to further interpret the results from the uptake experiments and presented in  
352 **Figure S5**. Simulations at pH 7 suggest that the cationic U aqueous species are prevalent in the  
353 *HDPA+U* reactors and in the *HDPA+U+Ca* reactors, with 70% (UO<sub>2</sub>)<sub>3</sub>(OH)<sub>5</sub><sup>+</sup>, 20%  
354 (UO<sub>2</sub>)<sub>5</sub>(OH)<sub>7</sub><sup>+</sup> and 6% UO<sub>2</sub>OH<sup>+</sup>. Anionic U aqueous species are prevalent in the *HDPA+U+CO<sub>3</sub>*  
355 reactors, with 75% UO<sub>2</sub>(CO<sub>3</sub>)<sub>3</sub><sup>-4</sup> and 21% UO<sub>2</sub>(CO<sub>3</sub>)<sub>2</sub><sup>-2</sup>. For the *HDPA+U+Ca+CO<sub>3</sub>* reactors,  
356 67% Ca<sub>2</sub>UO<sub>2</sub>(CO<sub>3</sub>)<sub>3</sub> neutral U species and 31% CaUO<sub>2</sub>(CO<sub>3</sub>)<sub>3</sub><sup>-2</sup> anionic U species were present.  
357 The presence of these ternary calcium-uranyl-carbonate aqueous complexes has also been  
358 reported in other studies.<sup>7, 34, 50</sup> As our experiments are conducted at pH 7 > pK<sub>a</sub>=2.6 for HDPA,  
359 the surface is negatively charged, causing electrostatic repulsion with the negative and neutral  
360 aqueous complexes. This would prevent U binding with the HDPA surface and resulting in lower  
361 uptake for *HDPA+U+CO<sub>3</sub>* and *HDPA+U+Ca+CO<sub>3</sub>* reactors. Additional extraction experiments  
362 with targeted reactants were pursued to better understand the U release to solution from surface  
363 associated U species on the reacted mats.

364

### 365 **3.4 Extractions experiments**

366 Higher U release from the HDPA reacted mats was observed after extractions with HCO<sub>3</sub>  
367 compared to MgCl<sub>2</sub>, indicating that the U associated to these mats is more amenable to  
368 complexation rather than ion exchange. The results from the extraction experiments are

369 presented in **Figure 3**. The *reacted HDPA+U* mats had 70% higher U release (3.0  $\mu\text{g HCO}_3$   
370 extractable U) with extractions using  $\text{HCO}_3$  when compared to  $\text{MgCl}_2$  extractions (0.9  $\mu\text{g MgCl}_2$   
371 extractable U). A similar trend was observed for the *reacted HDPA+U+Ca* mats, given that 78%  
372 higher  $\text{HCO}_3$  extractable U (3.9  $\mu\text{g}$ ) was released when compared to  $\text{MgCl}_2$  extractable U (0.8  
373  $\mu\text{g}$ ). An order of magnitude higher  $\text{HCO}_3$  extractable U was obtained for the *reacted*  
374 *HDPA+U+CO<sub>3</sub>* mats (1.7  $\mu\text{g U}$ ) and *reacted HDPA+U+Ca+CO<sub>3</sub> reacted* mats (0.6  $\mu\text{g U}$ ) in  
375 contrast to that released from  $\text{MgCl}_2$  extractions (0.02  $\mu\text{g}$  for *reacted HDPA+U+CO<sub>3</sub> reacted*  
376 mats and 0.06  $\mu\text{g}$  for *reacted HDPA+U+Ca+CO<sub>3</sub> mats*). This result suggests that U is initially  
377 complexed to the surface of the HDPA reacted mats after the uptake experiments, but then is  
378 removed from the surface and released to solution after complexation with bicarbonate upon  
379 extraction at pH 8.3.

380 Although the *HDPA+U+CO<sub>3</sub>* and *HDPA+U+Ca+CO<sub>3</sub>* reactors had lower U uptake, most  
381 extractable U was amenable to complexation after  $\text{HCO}_3$  addition. The low U released after  
382 extractions with  $\text{MgCl}_2$  indicates limited ion exchangeable U in these mats. Strong complexing  
383 agents such as  $\text{HCO}_3^-$  would bind and solubilize most surface associated U complexes<sup>1, 42, 51</sup>  
384 resulting in release of both the inner sphere and outer sphere surface U complexes into solution.  
385 Thus, a higher  $\text{HCO}_3^-$  and low  $\text{MgCl}_2$  extractible U support the presence of inner-sphere U  
386 surface complex on all the reacted mats.

387

### 388 **3.5 Solid analyses**

389 Further analyses of the reacted mats were carried out using XAS, XPS and SERS to  
390 understand the binding structure of surface associated U. The EXAFS U L-III spectra (**Figure 4**)  
391 shows that all the reacted mats had a similar shape to each other, with no matches to the

392 reference compounds. To understand the structural motif of the surface associated uranyl, shell-  
393 by-shell fitting (**Figure 5**) for *reacted HDPA+U mat* was conducted. The fitting of peaks  
394 observed in the Fourier Transformed EXAFS spectra (**Figure 4b, Figure 5**) around 1.78 Å  
395 corresponds to the two U=O dioxo bonds and five U-O bonds with atomic distances of 2.30 Å.  
396 The FT peaks at 2.3 Å is likely due to shell of neighboring atoms, which in our system is nitrate  
397 ligands, at atomic distance of 2.88 Å. The FT peaks observed from 2.9 to 3.1 Å can be attributed  
398 to a second neighbor shell of U-P coordination on HDPA, which suggests inner-sphere  
399 complexation through one of the hydroxide of the phosphonic acid functional group ( $\equiv\text{P-O-U}$ ,  
400 atomic distance U-P 3.58 Å). Comparable atomic distances for surface associated U have been  
401 reported in literature.<sup>52-54</sup> The similar EXAFS spectra for all other reacted mats (*HDPA+U+Ca*,  
402 *HDPA+U+CO<sub>3</sub>*, *HDPA+U+Ca+CO<sub>3</sub>*) indicates that the U binding on surface was consistent to  
403 the *HDPA+U* only shell-by-shell fitting. Thus, the U is present as a seven coordinated inner-  
404 sphere complex (UO<sub>2</sub>O<sub>5</sub>) with the HDPA mat as seen from the EXAFS shell-by-shell fitting.

405 The XPS survey scans and U 4*f* high-resolution spectra detected the presence of U in the near  
406 surface of all the reacted mats (**Table 1**). The U 4*f* high resolution spectra for all reacted mats  
407 had similar shapes which indicates similar U(VI) binding in the near surface (**Figure 6**). Fitting  
408 of the U 4*f*<sub>7/2</sub> spectra indicates the presence of two components with binding energy at 381.6 eV  
409 and 379.6 eV. A U 4*f* satellite peak is observed at 384.4 eV. The U 4*f*<sub>5/2</sub> spectra imitates the  
410 shape of the components of U 4*f*<sub>7/2</sub> with exactly 10.9 eV lower binding energy and one-third of  
411 the intensity.<sup>55</sup> Since these two components are present for all the reacted mats, the near surface  
412 associated uranyl species is likely the same. Analysis of high-resolution P 2*p* spectra indicate  
413 that there are no noticeable changes in shape for all the reacted mats. The lack of changes in the

414 EXAFS U L-III spectra and XPS U 4f high resolution spectra in all the reacted mats suggests that  
415 similar binding environment on the surface reacted HDPA mats in all reaction conditions.

416 SERS measurements with Au-MHA nanostars are utilized to determine uranyl complexes  
417 present on HDPA-PAN mat upon coordinating with uranyl and different ions based on molecular  
418 vibrational frequencies in the spectra. **Figure 7** shows SERS spectral deconvolution results for  
419 *reacted HDPA+U*, *HDPA+U+Ca*, *HDPA+U+CO<sub>3</sub>* mats suggest the presence of monodentate  
420 uranyl phosphonate species. No U signal was observed on *reacted HDPA+U+Ca+CO<sub>3</sub>* mats  
421 due to the low U uptake on the mats was below the detection limit of SERS. The identity of the  
422 associated uranyl complexed are assigned based on known vibrational frequency perturbations  
423 from carboxylate (from MHA) and phosphonate (from HDPA). While both functional groups  
424 induce a red-shift in the uranyl nitrate frequency, which is typically centered at  $870\pm 1$   $\text{cm}^{-1}$ , each  
425 functional group induces a specific red-shift that depends on the ligand denticity and systematic  
426 impacts on vibrational feature band width (estimated using full width at half maximum).  
427 Previously, it was shown that monodentate ( $\kappa^1$ ) coordination to carboxylate and phosphonate  
428 groups induce a red shift of  $11$   $\text{cm}^{-1}$  and bidentate ( $\kappa^2$ ) carboxylate coordination a  $20$   $\text{cm}^{-1}$  shift.<sup>56</sup>  
429 Thus, vibrational frequencies at  $859\pm 1$ ,  $847\pm 1$ ,  $838\pm 1$ , and  $828\pm 1$   $\text{cm}^{-1}$  are tentatively assigned  
430 as  $\text{UO}_2(\text{HDPA})(\text{NO}_3)_2^-$ ,  $\text{UO}_2(\text{HDPA})(\kappa^1\text{-COO})(\text{NO}_3)^-$ ,  $\text{UO}_2(\text{HDPA})(\kappa^1\text{-COO})_2^-$ , and  
431  $\text{UO}_2(\text{HDPA})(\kappa^1\text{-COO})(\kappa^2\text{-COO})^-$  complexes, respectively. As a result of the low U uptake in  
432 presence of bicarbonate, SERS spectra showed only one feature centered at  $829$   $\text{cm}^{-1}$  for  
433 *HDPA+U+CO<sub>3</sub>+HDPA* reacted mats, which can be tentatively assigned as  $\text{UO}_2(\text{HDPA})(\kappa^1\text{-}$   
434  $\text{COO})(\kappa^2\text{-CO}_3)$ . These assignments are supported by vibrational feature bandwidths assignments  
435 as these are impacted by the number and extent of electron donating ligands at the equatorial  
436 plane of uranyl cation.<sup>4, 38</sup> Specifically, previous studies<sup>5, 57</sup> showed the increased number of

437 ligands causes the vibrational band width to increase by  $2\text{ cm}^{-1}$  per ligand. Interestingly on all  
438 mat samples, the  $\text{UO}_2(\text{HDPA})$  complex that was observed via monodentate coordination  
439 remained intact despite the presence of nitrate, carboxylate, and carbonate groups. This suggests  
440 that the uranyl phosphonate complex has the largest stability constant among uranyl complexes  
441 present in solution and on the polymer surface.

442

### 443 **3.6 Mechanistic insights**

444 The results from this study indicate that U(VI) binding occurs primarily on the deprotonated  
445 oxygen of the phosphonate ( $\equiv\text{P-O}^-$ ). As the cationic U aqueous species would easily bind to the  
446 negatively charged  $\equiv\text{P-O}^-$  surface site, a higher U uptake was observed for the *HDPA+U* and  
447 *HDPA+U+Ca* reactors. The lower U uptake in the *HDPA+U+CO<sub>3</sub>* and *HDPA+U+Ca+CO<sub>3</sub>*  
448 reacted mats is due to the repulsion between anionic aqueous U species with the negatively  
449 charge phosphonate polymer surface. This limited U-uptake was confirmed by the minimal ion-  
450 exchangeable surface complexes. The surface associated U is predominantly an inner-sphere  
451 surface complex, as observed from the  $\text{HCO}_3^-$  extractions and EXAFS solid analyses. Finally,  
452 vibrational spectroscopy analysis suggests that U-phosphonate species are the most  
453 thermodynamically stable species present on the mats regardless of the initial U solution  
454 chemistry. The presence of this strongly complexed U-phosphonate for all the solution  
455 conditions indicate selective U uptake as reported in uranium-phosphonates literature.<sup>31, 36, 58</sup>  
456 Thus, the surficial interaction of aqueous U species strongly influences the total U uptake on the  
457 solid electrospun polymer.

458

### 459 **3.7 Conclusions**

460 Uranium remains a persistent water quality problem for many drinking water consumers  
461 reliant on groundwater as a source in the arid southwestern United States. There remain  
462 opportunities for technological advances that can improve access to reliable methods for uranium  
463 detection and treatment. Outcomes of the current work help to improve our understanding of the  
464 fabrication and performance of a promising material class, functionalized electrospun polymers,  
465 that could be integrated into sensing and treatment applications.<sup>4, 25</sup>

466 For functionalized polymer fabrication, we find that longer chain alkyl phosphonates  
467 perform best for U uptake. We attribute this behavior to their inherent nature to segregate at the  
468 air-polymer interface during electrospinning, and, most importantly, their better retention within  
469 the polymer nanofiber matrix during application. More work is needed to better understand the  
470 nature of the surfactant-polymer interaction responsible for the better retention of HDPA and  
471 ODPA, and whether this observation is more broadly applicable to other types of surfactants  
472 integrated into other types of electrospun polymers.

473 Related to phosphonate-functionalized nanofiber polymer performance, the presence of  
474 environmentally relevant concentrations of Ca and CO<sub>3</sub> inhibits U uptake in phosphonate  
475 functionalized electrospun polymers. Using spectroscopic methods, we identified the mechanism  
476 of U uptake as inner-sphere complexation with U-phosphonate monodentate surface complexes,  
477 which were observed on all the reacted mats. Ultimately, given their modest uptake, we envision  
478 that these functionalized nanofiber membranes may be better suited for applications in sensing  
479 rather than treatment, where the stability of inner-sphere complexation as a binding mechanism  
480 will be desirable for highly specific binding in complex environmental or biological matrices.

481

482 **Acknowledgements**

483 This work was supported by the U.S. National Institute of Environmental Health Science  
484 (NIEHS) under award number R01ES027145 and UNM METALS Superfund Research Program  
485 Center P42ES025589 and University of Iowa Superfund Research Program Center  
486 P42ES013661. The authors would like to acknowledge Margaret E. Carolan for assistance with  
487 U uptake experiments and U analysis. We also acknowledge the NIEHS K.C. Donnelly  
488 Externship Award Supplement which supported Nabil Shaikh to perform experiments at the  
489 University of Iowa. AJH's acknowledges the IR/D (Individual Research and Development)  
490 program associated with her appointment at the National Science Foundation. Use of the SSRL  
491 Stanford Synchrotron Radiation Lightsource, SLAC National Accelerator Laboratory, is  
492 supported by the U.S. Department of Energy, Office of Science, Office of Basic Energy Sciences  
493 under Contract No. DE-AC02-76SF00515.

494 **Tables & Figures**

495

496 **Table 1.** XPS survey scans indicating the atomic composition in the near surface.

	<b>C1s%</b>	<b>N1s%</b>	<b>O1s%</b>	<b>P2p%</b>	<b>U4f%</b>	<b>Na1s%</b>	<b>Ca2p%</b>
<b>HDPa control</b>	<b>80.6</b> ± 0.98	<b>8.4</b> ± 2.4	<b>9.7</b> ± 3.7	<b>1.3</b> ± 0.34	<b>n.d.</b>	<b>n.d.</b>	<b>n.d.</b>
<b>HDPa+U</b>	<b>79.5</b> ± 1.1	<b>12.7</b> ± 0.37	<b>6.5</b> ± 1.3	<b>0.4</b> ± 0.05	<b>0.2</b> ± 0.04	<b>0.7</b> ± 0.09	<b>n.d.</b>
<b>HDPa+U+Ca</b>	<b>78.8</b> ± 1.0	<b>12.6</b> ± 0.6	<b>7.5</b> ± 1.2	<b>0.4</b> ± 0.06	<b>0.2</b> ± 0.03	<b>0.2</b> ± 0.05	<b>0.2</b> ± 0.04
<b>HDPa+U+CO<sub>3</sub></b>	<b>79.9</b> ± 0.3	<b>14.4</b> ± 0.81	<b>4.4</b> ± 0.5	<b>0.4</b> ± 0.01	<b>0.1</b> ± 0.01	<b>0.7</b> ± 0.07	<b>n.d.</b>
<b>HDPa+U+Ca+CO<sub>3</sub></b>	<b>77.2</b> ± 0.2	<b>18.8</b> ± 0.24	<b>3.9</b> ± 0.06	<b>0.2</b> ± 0.04	<b>0.03</b> ± 0.02	<b>0.7</b> ± 0.07	<b>n.d.</b>

497

498

499

500

501

502

503

504

505

506

507

508

509

510

511

512

513

514

515

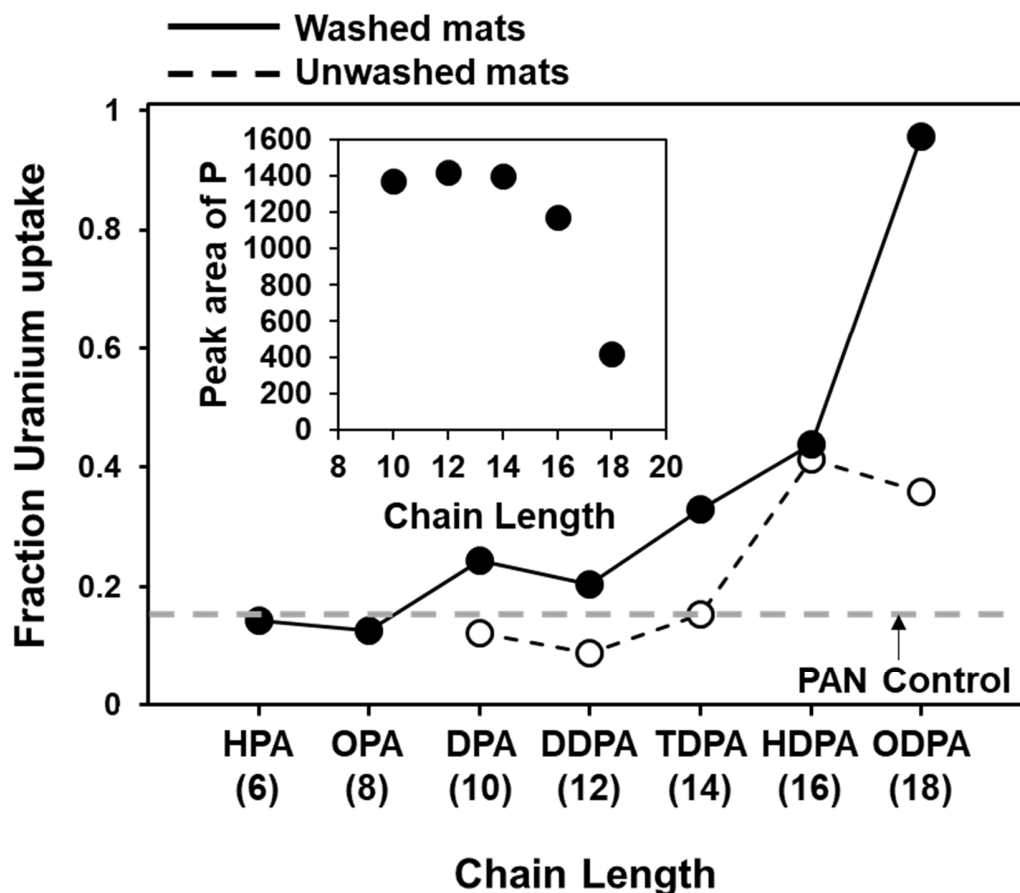
516

517

518

519

520

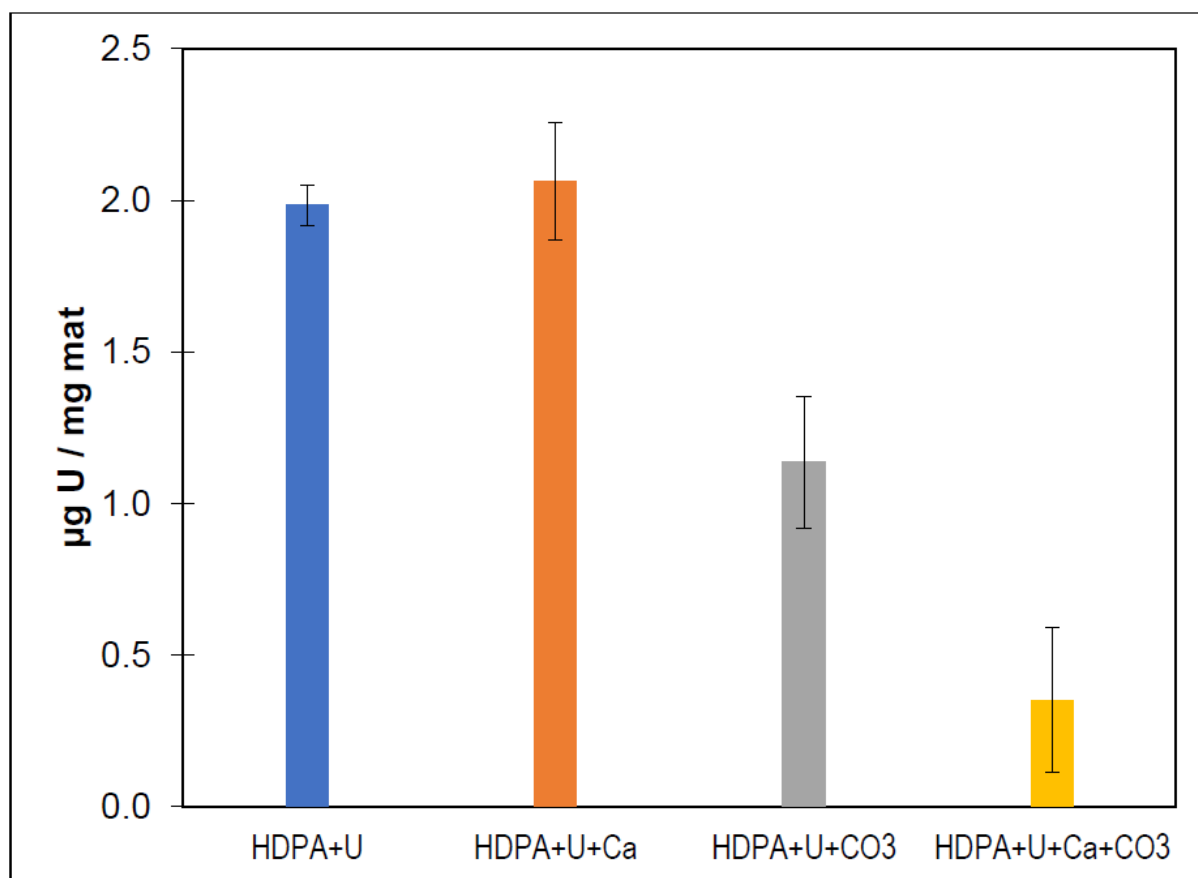


522

523 **Figure 1.** Effect of alkyl chain length on the fractional uranium (U) uptake by phosphonate-  
 524 functionalized PAN nanofibers. Data are shown for functionalized nanofibers reacted with 1  $\mu\text{M}$   
 525 U at pH 2 in 0.25 g/L sorbent systems for 16 h. Results are shown for materials used immediate  
 526 after synthesis (“unwashed”) and materials used after extensively rinsing with water to remove  
 527 loosely retained surfactant (“washed”). The U removal observed in control systems with  
 528 unfunctionalized PAN is shown as a dotted horizontal line. Bracketed numbers along the x-axis  
 529 indicate the alkyl phosphonate chain length. Error bars, if not visible, are smaller than the  
 530 symbols. The inset shows the response (based on the P 2p peak area) for P from XPS analysis of  
 531 unwashed materials (spectra are shown in Figure S3).

532

533

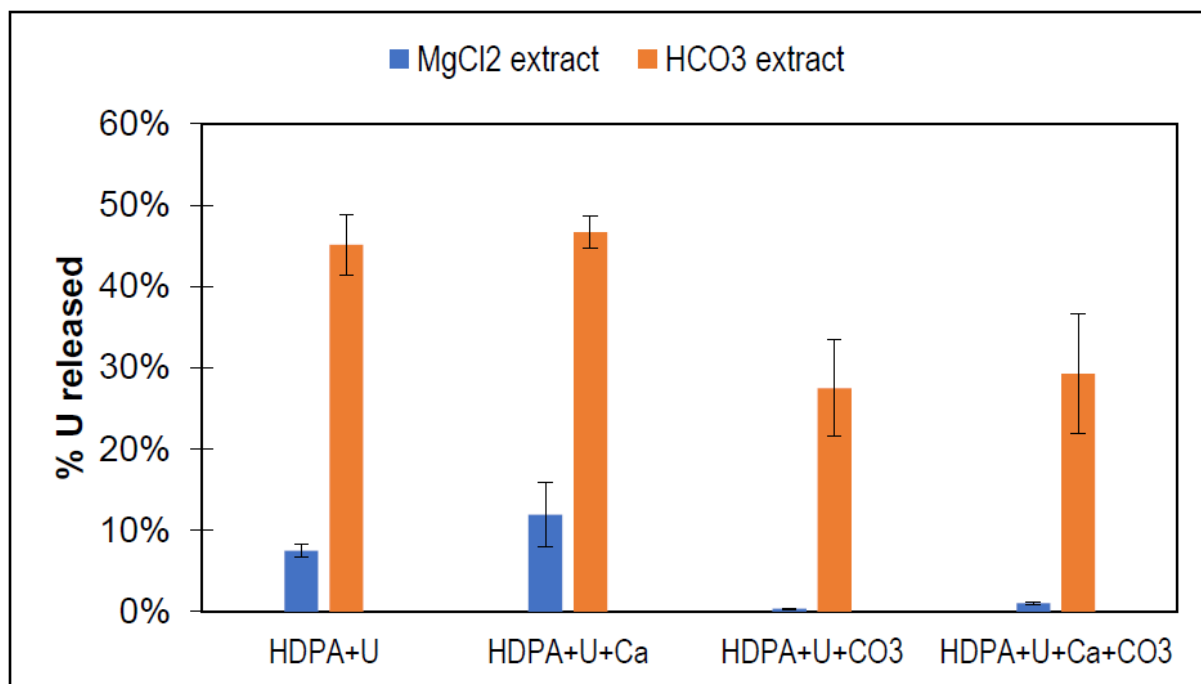


534

535

536 **Figure 2.** Uptake of U ( $\mu\text{g U / mg mat}$ ) on HDPA-PAN electrospun mats reacted with  $10 \mu\text{M}$   
 537 [U],  $50 \text{ mM}$  [HEPES] and in the presence of either  $5 \text{ mM}$  [Ca] (orange),  $5 \text{ mM}$  [CO<sub>3</sub>] (gray) or  
 538 both  $5 \text{ mM}$  [Ca] and [CO<sub>3</sub>] (yellow). The experiments were conducted using  $5 \text{ mg}$  mat in  $20 \text{ ml}$   
 539 solution reacted for  $16 \text{ hours}$ . Error bars represent the standard deviation of triplicate reactors.

540



541

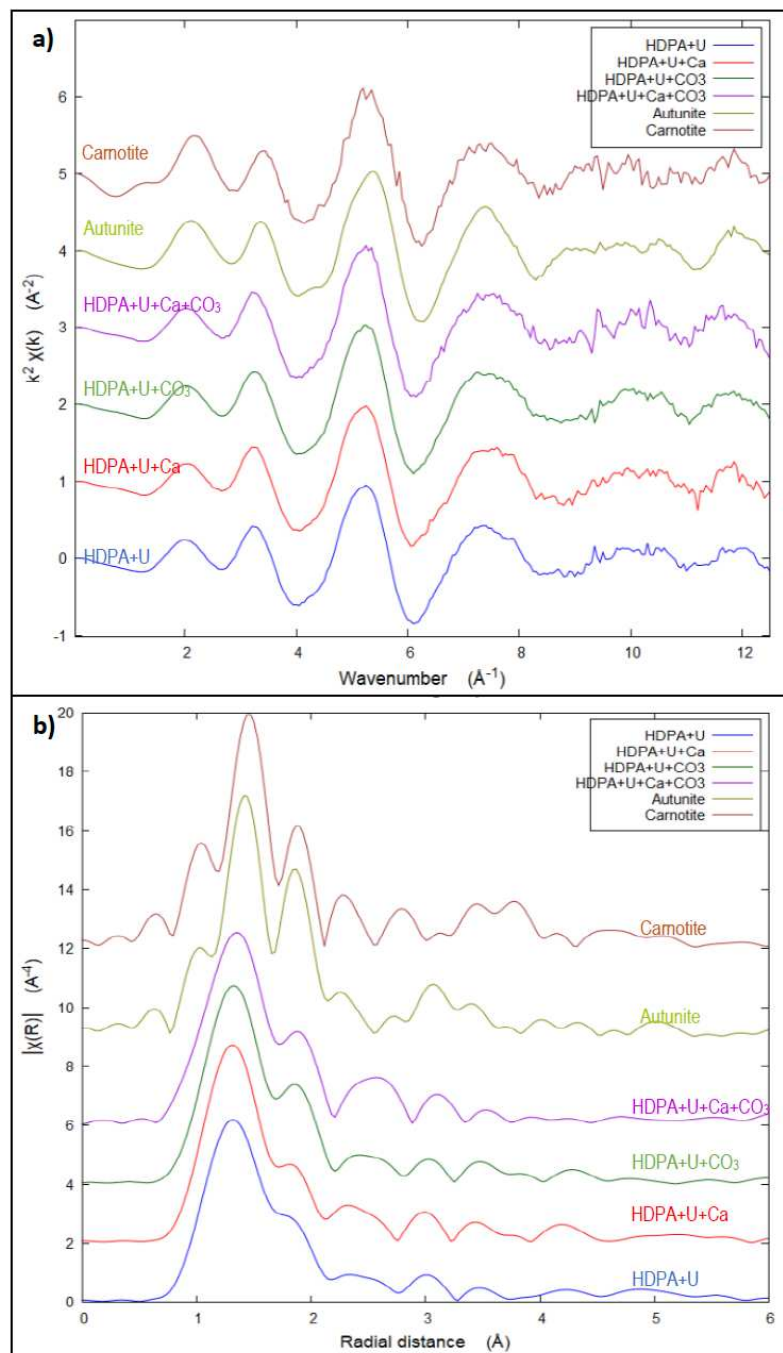
542 **Figure 3.** Results from reactivity experiments indicating % U released from the reacted mats  
543 after the addition of extractants (a) MgCl<sub>2</sub> (b) HCO<sub>3</sub>. Reaction conditions involved taking the  
544 reacted mats from U uptake experiments and reacting with each of the extractants.

545

546

547

548

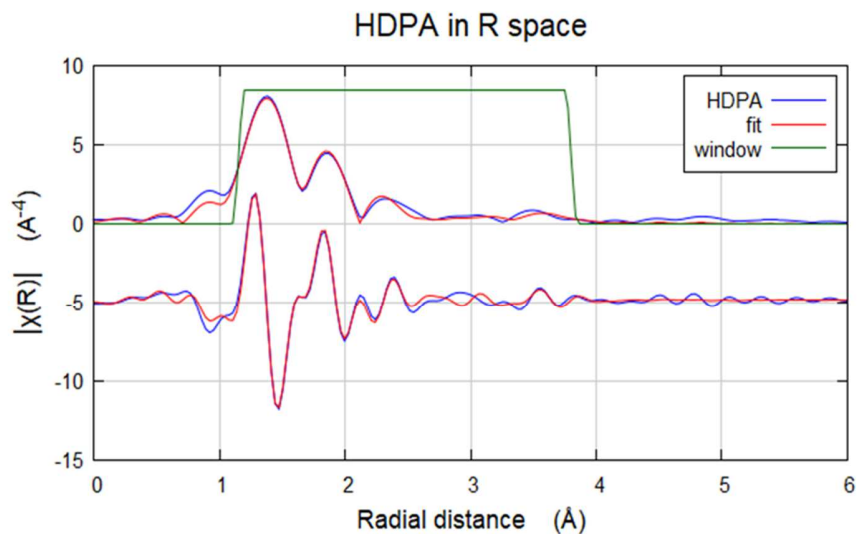


549

550

551 **Figure 4.** U LIII-edge EXAFS spectra from beamline 11-2 in (a) real-part (b) Fourier  
 552 transformed for reacted HDPA mats compared to references autunite and carnotite minerals.  
 553 Reaction conditions [U] = 10  $\mu\text{M}$ , Mat = 5 mg, volume = 20 ml, pH = 6.8 buffered HEPES =  
 554 10mM.

555



	N, Coordination no.	D, distance (Å)	$\sigma^2$ , mean square deviation (Å <sup>2</sup> )
<i>U-O<sub>axial</sub></i>	2	1.78(1)	0.0018(1)
<i>U-O<sub>equatorial</sub></i>	5	2.30(1)	0.008(1)
<b>U-N</b>	2	2.88(2)	0.003(2)
<b>U-O</b>	2	4.21(3)	0.006(3)
<b>U-P</b>	1	3.58(3)	0.004(3)

556

557

558

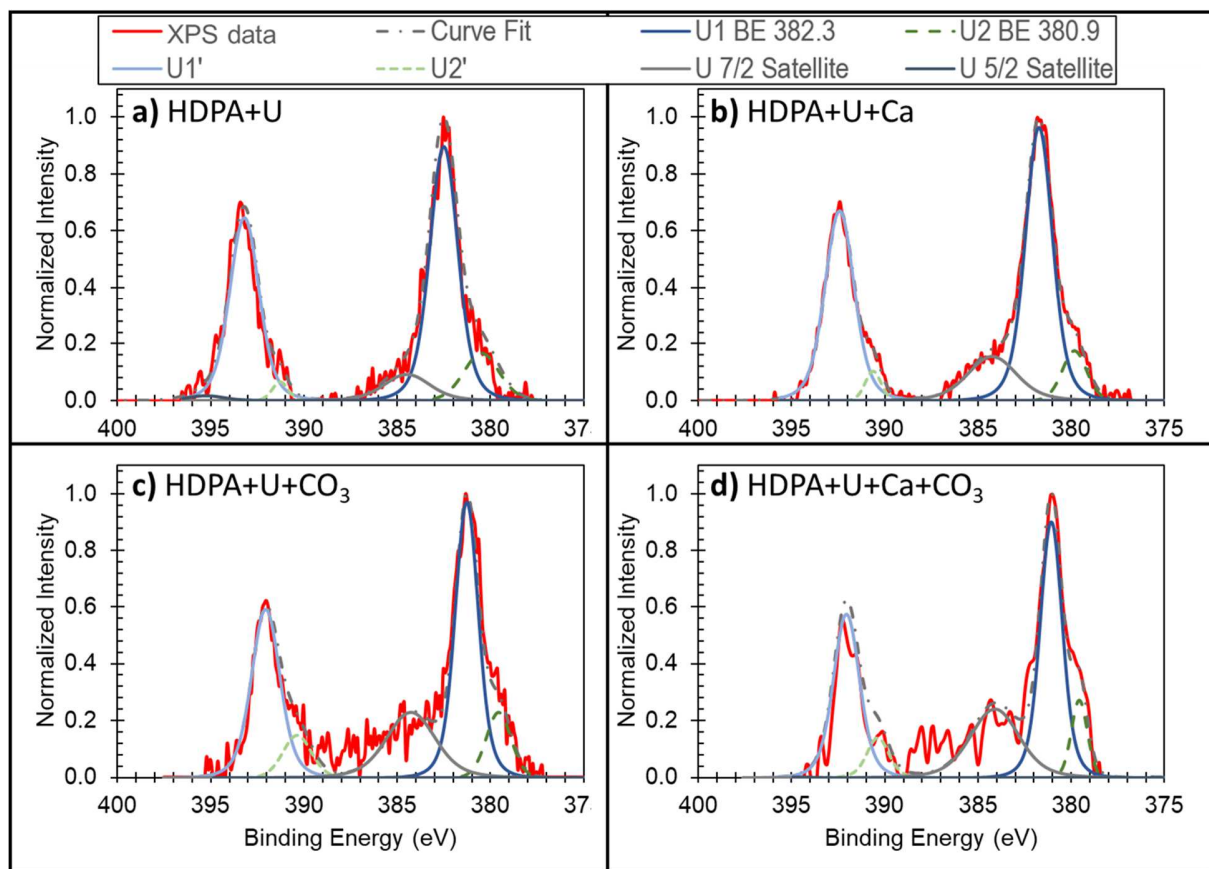
559 **Figure 5.** EXAFS shell-by-shell fitting results for HDDPA+U mat. Reaction conditions [U] = 10  
 560  $\mu$ M, Mat = 5 mg, volume = 20 ml, pH = 6.8 buffered HEPES = 10mM.

561

562

563

564

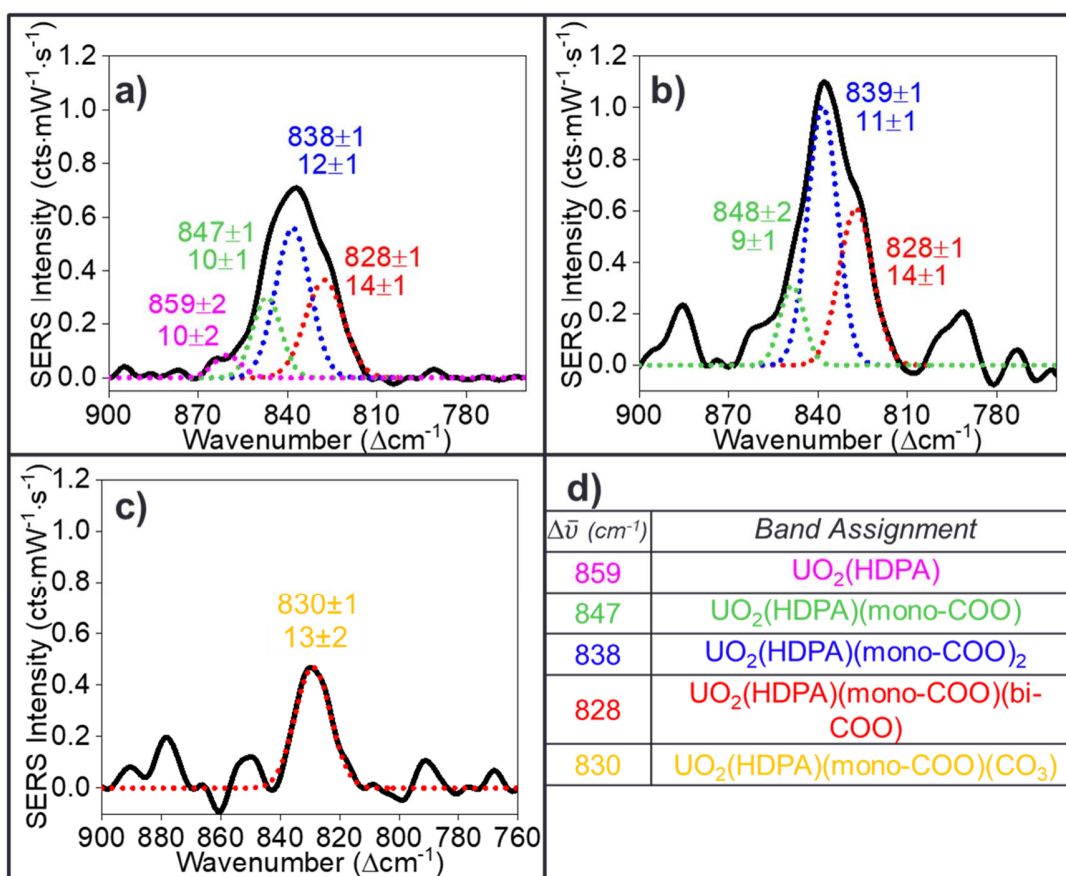


565

566

567 **Figure 6.** XPS High Resolution U 4f photo peak for reacted samples (red) and fittings of U 4f  
 568 components (inset) for reacted HDBA mats (a) 10  $\mu\text{M}$  U, (b) 10  $\mu\text{M}$  U+ 5 mM  $\text{Ca}^{2+}$ , (c) 10  $\mu\text{M}$  U  
 569 + 5 mM  $\text{CO}_3^{2-}$  and (d) 10  $\mu\text{M}$  U+ 5 mM  $\text{Ca}^{2+}$  + 5 mM  $\text{CO}_3^{2-}$ , from U uptake experiments.  
 570 Reaction conditions [U] = 10  $\mu\text{M}$ , Mat = 5 mg, volume = 20 ml, pH = 6.8 buffered HEPES =  
 571 10mM.

572



573  
 574  
 575  
 576 **Figure 7.** SERS spectra and deconvolution results on HDPA PAN mats incubated with (a) 10  
 577  $\mu M$  U, (b) 10  $\mu M$  U+ 5 mM  $Ca^{2+}$ , (c) 10  $\mu M$  U + 5 mM  $CO_3^{2-}$  and (d) shows detected uranyl-  
 578 HDPA complexes matched with vibrational frequencies obtained from the band deconvolution.

579

580

581

582

583 **References**

584  
585

- 586 1. S. Avasarala, P. C. Lichtner, A.-M. S. Ali, R. González-Pinzón, J. M. Blake and J. M.  
587 Cerrato, Reactive Transport of U and V from Abandoned Uranium Mine Wastes,  
588 *Environ. Sci. Technol.*, 2017, **51**, 12385-12393.
- 589 2. M. E. Harmon, J. Lewis, C. Miller, J. Hoover, A. S. Ali, C. Shuey, M. Cajero, S. Lucas,  
590 K. Zychowski, B. Pacheco, E. Erdei, S. Ramone, T. Nez, M. Gonzales and M. J. Campen,  
591 Residential proximity to abandoned uranium mines and serum inflammatory potential in  
592 chronically exposed Navajo communities, *J. Expo. Sci. Environ. Epidemiol.*, 2017, **27**,  
593 365-371.
- 594 3. J. Lewis, J. Hoover and D. MacKenzie, Mining and Environmental Health Disparities in  
595 Native American Communities, *Curr. Environ. Health Rep.*, 2017, **4**, 130-141.
- 596 4. G. Lu, A. J. Johns, B. Neupane, H. T. Phan, D. M. Cwiertny, T. Z. Forbes and A. J. Haes,  
597 Matrix-Independent Surface-Enhanced Raman Scattering Detection of Uranyl Using  
598 Electrospun Amidoximated Polyacrylonitrile Mats and Gold Nanostars, *Anal. Chem.*,  
599 2018, **90**, 6766-6772.
- 600 5. G. Lu, A. J. Haes and T. Z. Forbes, Detection and identification of solids, surfaces, and  
601 solutions of uranium using vibrational spectroscopy, *Coord. Chem. Rev.*, 2018, **374**, 314-  
602 344.
- 603 6. P. J. Lebed, J.-D. Savoie, J. Florek, F. Bilodeau, D. Larivière and F. Kleitz, Large Pore  
604 Mesostructured Organosilica-Phosphonate Hybrids as Highly Efficient and Regenerable  
605 Sorbents for Uranium Sequestration, *Chem. Mater.*, 2012, **24**, 4166-4176.
- 606 7. W. Dong and S. C. Brooks, Determination of the Formation Constants of Ternary  
607 Complexes of Uranyl and Carbonate with Alkaline Earth Metals ( $Mg^{2+}$ ,  $Ca^{2+}$ ,  $Sr^{2+}$ , and  
608  $Ba^{2+}$ ) Using Anion Exchange Method, *Environ. Sci. Technol.*, 2006, **40**, 4689-4695.
- 609 8. E. P. Horwitz, M. L. Dietz, R. Chiarizia, H. Diamond, A. M. Essling and D. Graczyk,  
610 Separation and preconcentration of uranium from acidic media by extraction  
611 chromatography, *Anal. Chim. Acta*, 1992, **266**, 25-37.
- 612 9. J. Qian, B. Jennings, David M. Cwiertny and A. Martinez, Emerging investigator series:  
613 development and application of polymeric electrospun nanofiber mats as equilibrium-  
614 passive sampler media for organic compounds, *Environ. Sci. Process. Impacts*, 2017, **19**,  
615 1445-1456.
- 616 10. J. J. Alcaraz-Espinoza, A. E. Chávez-Guajardo, J. C. Medina-Llamas, C. A. S. Andrade  
617 and C. P. de Melo, Hierarchical Composite Polyaniline–(Electrospun Polystyrene) Fibers  
618 Applied to Heavy Metal Remediation, *ACS Appl. Mater. Interfaces*, 2015, **7**, 7231-7240.
- 619 11. K. T. Peter, N. V. Myung and D. M. Cwiertny, Surfactant-assisted fabrication of porous  
620 polymeric nanofibers with surface-enriched iron oxide nanoparticles: composite filtration  
621 materials for removal of metal cations, *Environ. Sci. Nano*, 2018, **5**, 669-681.
- 622 12. L. Hu, X.-W. Yan, C.-G. Yao, S.-Y. Deng, X.-M. Gao, X.-J. Zhang and D. Shan,  
623 Preparation of amidoximated coaxial electrospun nanofibers for uranyl uptake and their  
624 electrochemical properties, *Sep. Purif. Technol.*, 2016, **171**, 44-51.
- 625 13. K. E. Greenstein, N. V. Myung, G. F. Parkin and D. M. Cwiertny, Performance  
626 comparison of hematite ( $\alpha$ - $Fe_2O_3$ )-polymer composite and core-shell nanofibers as point-  
627 of-use filtration platforms for metal sequestration, *Water Res.*, 2019, **148**, 492-503.

- 628 14. P. Singhal, B. G. Vats and V. Pulhani, Magnetic nanoparticles for the recovery of  
629 uranium from sea water: Challenges involved from research to development, *J. Ind. Eng.*  
630 *Chem.*, 2020, **90**, 17-35.
- 631 15. P. Singhal, B. G. Vats, A. Yadav and V. Pulhani, Efficient extraction of uranium from  
632 environmental samples using phosphoramidate functionalized magnetic nanoparticles:  
633 Understanding adsorption and binding mechanisms, *J. Hazard. Mater.*, 2020, **384**,  
634 121353.
- 635 16. K. Yoon, K. Kim, X. Wang, D. Fang, B. S. Hsiao and B. Chu, High flux ultrafiltration  
636 membranes based on electrospun nanofibrous PAN scaffolds and chitosan coating,  
637 *Polymer*, 2006, **47**, 2434-2441.
- 638 17. N. Horzum, T. Shahwan, O. Parlak and M. M. Demir, Synthesis of amidoximated  
639 polyacrylonitrile fibers and its application for sorption of aqueous uranyl ions under  
640 continuous flow, *Chem. Eng. J.*, 2012, **213**, 41-49.
- 641 18. S. Chatterjee and S. De, Adsorptive removal of arsenic from groundwater using a novel  
642 high flux polyacrylonitrile (PAN)-laterite mixed matrix ultrafiltration membrane,  
643 *Environ. Sci. Water Res. Technol.*, 2015, **1**, 227-243.
- 644 19. F. Huang, Y. Xu, S. Liao, D. Yang, Y.-L. Hsieh and Q. Wei, Preparation of Amidoxime  
645 Polyacrylonitrile Chelating Nanofibers and Their Application for Adsorption of Metal  
646 Ions, *Materials*, 2013, **6**, 969-980.
- 647 20. F. Sebesta, J. John, A. Motl and K. Stamberg, *Evaluation of polyacrylonitrile (PAN) as a*  
648 *binding polymer for absorbers used to treat liquid radioactive wastes*, United States,  
649 1995.
- 650 21. K. J. Gagnon, H. P. Perry and A. Clearfield, Conventional and Unconventional Metal-  
651 Organic Frameworks Based on Phosphonate Ligands: MOFs and UMOFs, *Chem. Rev.*,  
652 2012, **112**, 1034-1054.
- 653 22. J.-G. Mao, Structures and luminescent properties of lanthanide phosphonates, *Coord.*  
654 *Chem. Rev.*, 2007, **251**, 1493-1520.
- 655 23. J. Xie, R. Lv, H. Peng, J. Fan, Q. Tao, Y. Dai, Z. Zhang, X. Cao and Y. Liu, Phosphate  
656 functionalized poly(vinyl alcohol)/poly(acrylic acid) (PVA/PAA): an electrospinning  
657 nanofiber for uranium separation, *J. Radioanal. Nucl. Chem.*, 2020, **326**, 475-486.
- 658 24. Z. Zeng, S. Yang, L. Zhang and D. Hua, Phosphonate-functionalized polystyrene  
659 microspheres with controlled zeta potential for efficient uranium sorption, *RSC Adv.*,  
660 2016, **6**, 74110-74116.
- 661 25. A. Johns, J. Qian, M. E. Carolan, N. Shaikh, A. Peroutka, A. Seeger, J. M. Cerrato, T. Z.  
662 Forbes and D. M. Cwiertny, Functionalized electrospun polymer nanofibers for treatment  
663 of water contaminated with uranium, *Environ. Sci. Water Res. Technol.*, 2020, **6**, 622-  
664 634.
- 665 26. J. G. Lundin, P. N. Coneski, P. A. Fulmer and J. H. Wynne, Relationship between surface  
666 concentration of amphiphilic quaternary ammonium biocides in electrospun polymer  
667 fibers and biocidal activity, *React. Funct. Polym.*, 2014, **77**, 39-46.
- 668 27. Z. Piskula, T. Manszewski, M. Kubicki and S. Lis, The structure and spectroscopic  
669 characterization of  $\text{UO}_2^{2+}$  complexes with tetraethyl methylenediphosphonate in solution  
670 and in solid state, *J. Mol. Struct.*, 2012, **1011**, 145-148.
- 671 28. S. Vukovic, B. P. Hay and V. S. Bryantsev, Predicting Stability Constants for Uranyl  
672 Complexes Using Density Functional Theory, *Inorg. Chem.*, 2015, **54**, 3995-4001.

- 673 29. T. M. Budnyak, A. V. Strizhak, A. Gładysz-Płaska, D. Sternik, I. V. Komarov, D.  
674 Kołodyńska, M. Majdan and V. A. Tertykh, Silica with immobilized phosphinic acid-  
675 derivative for uranium extraction, *J. Hazard. Mater.*, 2016, **314**, 326-340.
- 676 30. P. Zhou and B. H. Gu, Extraction of oxidized and reduced forms of uranium from  
677 contaminated soils: Effects of carbonate concentration and pH, *Environ. Sci. Technol.*,  
678 2005, **39**, 4435-4440.
- 679 31. J. D. Kubicki, G. P. Halada, P. Jha and B. L. Phillips, Quantum mechanical calculation of  
680 aqueous uranium complexes: carbonate, phosphate, organic and biomolecular species,  
681 *Chem. Cent. J.*, 2009, **3**, 10.
- 682 32. J. M. Blake, C. L. De Vore, S. Avasarala, A.-M. Ali, C. Roldan, F. Bowers, M. N. Spilde,  
683 K. Artyushkova, M. F. Kirk, E. Peterson, L. Rodriguez-Freire and J. M. Cerrato, Uranium  
684 mobility and accumulation along the Rio Paguante, Jackpile Mine in Laguna Pueblo, NM,  
685 *Environ. Sci. Process. Impacts*, 2017, **19**, 605-621.
- 686 33. Z. Pan, D. E. Giammar, V. Mehta, L. D. Troyer, J. G. Catalano and Z. Wang, Phosphate-  
687 Induced Immobilization of Uranium in Hanford Sediments, *Environ. Sci. Technol.*, 2016,  
688 **50**, 13486-13494.
- 689 34. G. Bernhard, G. Geipel, T. Reich, V. Brendler, S. Amayri and H. Nitsche, Uranyl(VI)  
690 carbonate complex formation: Validation of the  $C_a2UO_2(CO_3)_3(aq)$  species, *Radiochim.*  
691 *Acta*, 2001, **89**, 511-518.
- 692 35. B. Nowack and A. T. Stone, The Influence of Metal Ions on the Adsorption of  
693 Phosphonates onto Goethite, *Environ. Sci. Technol.*, 1999, **33**, 3627-3633.
- 694 36. B. Nowack, Environmental chemistry of phosphonates, *Water Res.*, 2003, **37**, 2533-2546.
- 695 37. D. M. Singer, K. Maher and G. E. Brown, Uranyl-chlorite sorption/desorption:  
696 Evaluation of different U(VI) sequestration processes, *Geochim. Cosmochim. Acta*, 2009,  
697 **73**, 5989-6007.
- 698 38. G. Lu, T. Z. Forbes and A. J. Haes, SERS detection of uranyl using functionalized gold  
699 nanostars promoted by nanoparticle shape and size, *Analyst*, 2016, **141**, 5137-5143.
- 700 39. G. Lu, T. Z. Forbes and A. J. Haes, Evaluating Best Practices in Raman Spectral Analysis  
701 for Uranium Speciation and Relative Abundance in Aqueous Solutions, *Anal. Chem.*,  
702 2016, **88**, 773-780.
- 703 40. H. T. Phan and A. J. Haes, Impacts of pH and Intermolecular Interactions on Surface-  
704 Enhanced Raman Scattering Chemical Enhancements, *J. Phys. Chem. C*, 2018, **122**,  
705 14846-14856.
- 706 41. D. V. Kravchuk, A. Blanes Diaz, M. E. Carolan, E. A. Mpundu, D. M. Cwiertny and T.  
707 Z. Forbes, Uranyl Speciation on the Surface of Amidoximated Polyacrylonitrile Mats,  
708 *Inorg. Chem.*, 2020, **59**, 8134-8145.
- 709 42. J. M. Blake, S. Avasarala, K. Artyushkova, A.-M. S. Ali, A. J. Brearley, C. Shuey, W. P.  
710 Robinson, C. Nez, S. Bill, J. Lewis, C. Hirani, J. S. L. Pacheco and J. M. Cerrato,  
711 Elevated Concentrations of U and Co-occurring Metals in Abandoned Mine Wastes in a  
712 Northeastern Arizona Native American Community, *Environ. Sci. Technol.*, 2015, **49**,  
713 8506-8514.
- 714 43. A. Tessier, P. G. C. Campbell and M. Bisson, Sequential extraction procedure for the  
715 speciation of particulate trace metals, *Anal. Chem.*, 1979, **51**, 844-851.
- 716 44. T. P. O'Connor and D. R. Kester, Adsorption of copper and cobalt from fresh and marine  
717 systems, *Geochim. Cosmochim. Acta*, 1975, **39**, 1531-1543.

- 718 45. D. A. Elias, J. M. Senko and L. R. Krumholz, A procedure for quantitation of total  
719 oxidized uranium for bioremediation studies, *J. Microbiol. Methods*, 2003, **53**, 343-353.
- 720 46. K. T. Peter, A. J. Johns, N. V. Myung and D. M. Cwiertny, Functionalized polymer-iron  
721 oxide hybrid nanofibers: Electrospun filtration devices for metal oxyanion removal,  
722 *Water Res.*, 2017, **117**, 207-217.
- 723 47. Y.-L. Wang, L. Zhu, B.-L. Guo, S.-W. Chen and W.-S. Wu, Mesoporous silica SBA-15  
724 functionalized with phosphonate derivatives for uranium uptake, *New J. Chem.*, 2014, **38**,  
725 3853-3861.
- 726 48. A. Kowal-Fouchard, R. Drot, E. Simoni and J. J. Ehrhardt, Use of Spectroscopic  
727 Techniques for Uranium(VI)/Montmorillonite Interaction Modeling, *Environ. Sci.*  
728 *Technol.*, 2004, **38**, 1399-1407.
- 729 49. C. Tournassat, R. M. Tinnacher, S. Grangeon and J. A. Davis, Modeling uranium(VI)  
730 adsorption onto montmorillonite under varying carbonate concentrations: A surface  
731 complexation model accounting for the spillover effect on surface potential, *Geochim.*  
732 *Cosmochim. Acta*, 2018, **220**, 291-308.
- 733 50. A. S. Saleh, J.-Y. Lee, Y. Jo and J.-I. Yun, Uranium(VI) sorption complexes on silica in  
734 the presence of calcium and carbonate, *J. Environ. Radioact.*, 2018, **182**, 63-69.
- 735 51. J. M. Blake, S. Avasarala, A.-M. S. Ali, M. Spilde, J. S. Lezama-Pacheco, D. Latta, K.  
736 Artyushkova, A. G. Ilgen, C. Shuey, C. Nez and J. M. Cerrato, Reactivity of As and U  
737 co-occurring in Mine Wastes in northeastern Arizona, *Chem. Geol.*, 2019, **522**, 26-37.
- 738 52. J. R. Bargar, R. Reitmeyer, J. J. Lenhart and J. A. Davis, Characterization of U(VI)-  
739 carbonato ternary complexes on hematite: EXAFS and electrophoretic mobility  
740 measurements, *Geochim. Cosmochim. Acta*, 2000, **64**, 2737-2749.
- 741 53. S. Rihs, C. Gaillard, T. Reich and S. J. Kohler, Uranyl sorption onto birnessite: A surface  
742 complexation modeling and EXAFS study, *Chem. Geol.*, 2014, **373**, 59-70.
- 743 54. H. A. Thompson, G. E. Brown and G. A. Parks, XAFS spectroscopic study of uranyl  
744 coordination in solids and aqueous solution, *Am. Mineral.*, 1997, **82**, 483-496.
- 745 55. E. S. Ilton and P. S. Bagus, XPS determination of uranium oxidation states, *Surf.*  
746 *Interface Anal.*, 2011, **43**, 1549-1560.
- 747 56. F. Quilès and A. Burneau, Infrared and Raman spectroscopic study of uranyl complexes:  
748 hydroxide and acetate derivatives in aqueous solution, *Vib. Spectrosc.*, 1998, **18**, 61-75.
- 749 57. C. Ruan, W. Luo, W. Wang and B. Gu, Surface-enhanced Raman spectroscopy for  
750 uranium detection and analysis in environmental samples, *Anal. Chim. Acta*, 2007, **605**,  
751 80-86.
- 752 58. W. Yang, T. G. Parker and Z.-M. Sun, Structural chemistry of uranium phosphonates,  
753 *Coord. Chem. Rev.*, 2015, **303**, 86-109.

754  
755

756